Engineered small extracellular vesicles as a FGL1/PD-L1 dual-targeting delivery system for alleviating immune rejection

Hsiang-i Tsai[2,*], Yingyi Wu[1,*], Xiaoyan Liu[1,*], Zhanxue Xu[1], Longshan Liu[3], Yisheng Huang[4], Linglu Wang[1], Weixian Zhang[1], Huanxi Zhang[3] , Dandan Su[1], Fahim Ullah Khan[5], Changxi Wang[3], John E. Eriksson[6], Bo Jia[4,#], Fang Cheng[1,#], Hongbo Chen[1,#]

1. School of Pharmaceutical Sciences (Shenzhen), Sun Yat-sen University, Shenzhen 518107, P.R. China
2. Department of Medical Imaging, The Affiliated Hospital of Jiangsu University, Zhenjiang 212001, China
3. Organ Transplant Center， The First Affiliated Hospital, Sun Yat-sen University, 58 Zhongshan 2nd Road, Guangzhou, Guangdong 510080, China.
4. Department of Oral Surgery, Stomatological Hospital, Southern Medical University, Guangzhou 510280, Guangdong, PR China
5. Zoology Department UST, Bannu Kp 28100, Pakistan
6. Cell Biology, Biosciences, Faculty of Science and Engineering, Åbo Akademi University, FI-20520, Turku, Finland; Turku Centre for Biotechnology, University of Turku and Åbo Akademi University, FI-20521, Turku, Finland.

[#]Corresponding author. Tel: +86 15071561390; E-mail: hysxuexi@163.com

[##]Corresponding author. Tel: +86 18123846151; E-mail: chengf9@mail.sysu.edu.cn

[###]Corresponding author. Tel: +86 15889353410; E-mail: chenhb7@mail.sysu.edu.cn

[*]These authors contributed equally to this work

Abstract

There is an urgent need for developing new immunosuppressive agents due to the toxicity of long-term use of broad immunosuppressive agents post organ transplantation. Comprehensive sample analysis revealed dysregulation of FGL1/LAG-3 and PD-L1/PD-1 immune checkpoints in allogenic heart transplantation mice and clinical kidney transplant patients. In order to enhance these two immunosuppressive signal axes, we developed a bioengineering strategy to simultaneously display FGL1/PD-L1 (FP) on the surface of small extracellular vesicles (sEVs). Among various cell sources, FP sEVs derived from mesenchymal stem cells (MSCs) not only enriched FGL1/PD-L1 expression, but also maintained the immunomodulatory properties of unmodified MSC sEVs. Next, we confirmed that FGL1 and PD-L1 on sEVs specifically bound to their receptors LAG-3 and PD-1 on target cells. Importantly, FP sEVs significantly inhibited T cell activation and proliferation *in vitro* and in a heart allograft model. Furthermore, FP sEVs encapsulated with low-dose FK506 (FP sEVs@FK506) exerted stronger effects on inhibiting T cell proliferation, reducing $CD8^+$ T cell density and cytokine production in the spleens and heart grafts, inducing regulatory T cells in lymph nodes, and extending graft survival. Taken together, dual-targeting sEVs has the potential to boost the immune inhibitory signalings in synergy and slow down transplant rejection.

Key words: Immunosuppressant; FGL1; PD-L1; Extracellular vesicles; Immunological rejection

Introduction

Immunosuppressants such as calcineurin inhibitor FK506 (Tacrolimus) or cyclosporin A (CsA) are widely used in organ transplantation [1-4]. Their prolonged use however, can result in a multitude of side effects, including infection, bone marrow suppression, and gastrointestinal reactions [5-8]. There is therefore an unmet need for the development of drugs based on novel mechanisms and targets to replace, or use in concert with, conventional immunosuppressive drugs, in order to enhance the overall survival rate of patients.

T-cell expressed immune checkpoints (ICPs) such as PD-1, TIM-3, VISTA, TIGIT and LAG-3 interact with their inhibitory ligands expressed on antigen presenting cells and/or on tumor cells, responsible for maintaining self-tolerance and preventing an autoimmune response [9-12]. Immune checkpoint inhibitors have been recently reported as an effective strategy for blocking these immunosuppressive axes, thereby overcoming tumor immune evasion[13]. Bispecific antibodies are also important in this regard, and have been demonstrated to interrupt a number of these axes (e.g. CTLA-4/CD80, PD-1/PD-L1), resulting in excellent therapeutic effects against malignant tumors [14-16]. These success highlights the feasibility to develop therapeutics to enhance the ICPs and thus suppress autoimmunity and other undesired immune responses. The immunosuppressive effect of ICP agonist antibodies have been demonstrated in the graft-versus-host disease and autoimmune disease models, but it is technically challenging to develop bispecific ICP agonist antibodies to restore immune tolerance [17].

In recent years, cell membrane-based nanovesicle delivery systems that readily display transmembrane proteins such as ICPs, have seen substantial development [18, 19]. We previously engineered cell membrane-derived nanovesicles (NVs) displaying PD-L1/CTLA-4 dual-targeting cargos. These NVs consequently enhanced PD-L1/PD-1 and CTLA-4/CD80 immune inhibitory pathways, exerted immune inhibitory effects, and prolonged the survival of mouse skin and heart grafts [20]. However, CTLA-4 binds to CD80 or CD86 on antigen-presenting cells (APCs) rather than T cells, and operates at different stages and locations of immune inhibition than the PD-L1 pathway [21, 22]. Furthermore, NVs are generated by serial

extrusion of cell membrane, leading to the membrane incompleteness, inner and outer membrane turnover, and incorrect arrangement of membrane molecules during preparation [20]. In contrast, small extracellular vesicles (sEVs), a 50–150 nm membrane vesicle containing miRNAs and proteins, have been identified as a superior alternative to natural membrane delivery systems [23-26] largely due to their high biocompatibility and negligible side effects. Interestingly, melanoma cells are reported to secrete sEVs carrying high level of PD-L1 and effectively suppress $CD8^+$ T cell activity [27]. Thus, combinational inhibition of both PD-1 and other ICPs on T cells by using sEVs simultaneously carrying multiple target ligands might be a more potent therapeutic strategy for attenuating T-cell mediated immune rejections.

Mesenchymal stem cells (MSCs) have been increasingly used for autoimmune disease treatment due to their immune modulation functions [28]. Recently, it was determined that MSCs exert their immune-modulatory effects, mostly by secreting soluble factors and sEVs [29, 30]. MSC derived sEVs have been reported to have therapeutic effects after organ transplantation and Graft-versus-host disease (GvHD), including immunosuppression, anti-inflammatory properties and the induction of tissue regeneration [31-34]. These favorable characteristics underscore the potential of MSC-sEVs as promising target vehicles to foster immune tolerance.

In this study, we first identified a simultaneous rise of PD-1 and LAG-3, but not their partner proteins PD-L1 and FGL1 in heart transplantation models and clinical kidney transplant patients. We then bioengineered MSCs to obtain sEVs simultaneously displaying highly surface FGL1/PD-L1, and confirmed their specificity to bind their ligands LAG-3 and PD-1 on T cells. The FGL1/PD-L1 dual-targeting sEVs (FP sEVs) inhibited the activation of T cells both *in vitro* and in a mouse heart transplantation model, via enhancing the immunosuppressive pathways of both FGL1/LAG-3 and PD-L1/PD-1. Importantly, FP sEVs encapsulated with FK506 displayed stronger inhibition of T cell proliferation than FP sEVs or FK506 alone *in vitro* and *in vivo*, providing strong evidence for a synergistic effect between low-dose FK506 and sEVs expressing FGL1/PD-L1 leading to the weakened alloimmune response and induced allograft tolerance. This constitutes a novel strategy for development of multi-targeting genetically

engineered sEVs as effective immunosuppressants to inhibit post-transplant rejection.

Methods and materials

Clinical samples of kidney transplant patients.

Nineteen kidney transplant recipients were enrolled in this study. They were divided into three groups: stable group (n = 7), antibody-mediated rejection (ABMR) group (n = 6), and T cell-mediated rejection (TCMR) group (n = 6). Approximately 20 mL of heparinized peripheral blood was obtained after allograft transplantation from patients. All patients gave informed consent for this study, which was approved by the Organ Transplant Center at the First Affiliated Hospital of Sun Yat-sen University (Clinical Trials. gov NO. 2019-456). Refer to previously published articles for the demographic clinical characteristics of the study in kidney transplant patients[35] . Information of patients involved in the experiments are listed in the Supplementary Table 1

Biochemicals and Antibodies.

Puromycin was purchased from Sigma-Aldrich. GAPDH, β-actin, GFP, OFP, SHP2, p-LCK, LCK, p-AKT (Thr308), AKT, p-ZAP70, and ZAP70 antibodies for western blot were purchased from Abmart. FGL1 antibodies were purchased from Santa Cruz Biotechnology Inc. Antibodies, including Human PD-L1 and PD-1 were purchased from Invitrogen. Human LAG-3 and Na^+K^+ATPase antibodies were purchased from Cell Signaling Technology and Santa Cruz Biotechnology Inc. respectively. Marker antibodies for exosomes, including anti-CD9, anti-CD63, and anti-ALIX, were purchased from Santa Cruz Biotechnology Inc, and anti-CD81 from System Biosciences. Wheat Germ Agglutinin (WGA) Alexa Fluor 488 and 350 dyes were purchased from Thermo Scientific. Ficoll Paque Plus used for isolating peripheral blood mononuclear cells (PBMC) cells was purchased from GE Healthcare. Staining antibodies, including CD3, CD4, CD8, CD25, and Foxp3 for FACS analysis were purchased from Biolegend Inc.

Cell lines and Cell cultures.

HEK-293T cells (human embryonic kidney cell lines), Jurkat cells (human acute T cell leukemia cell lines), HepG2 cells (human liver cancer cell lines), and A549 cells (human lung cancer cell lines) were purchased from American Type Culture Collection (ATCC). Cells were cultured in RPMI 1640 or DMEM supplemented with 10% fetal bovine serum (Gibco), 100 units/mL penicillin, and 100 μg/mL streptomycin, and were incubated at 37 °C in a 5% CO_2 atmosphere.

Plasmids and stable cell lines.

Plasmids from human (pLV-puro-TM-FGL1-GFPSpark), (pLV-puro-PD-L1-OFPSpark), (pLV-puro-PD-1-GFPSpark), and (pLV-puro-LAG-3-OFPSpark) and plasmids from mouse (pLV-puro-TM-FGL1-GFPSpark), and pLV-puro-mPD-L1-OFPSpark) were purchased from Sino Biological Inc. For stable cell lines, HEK-293T cells were transfected with packaging, envelope, and target plasmids using Lipo 3000 (ThermoFisher, Waltham, USA). Fluid change was performed at 12 h and at 24, 48, and 72 h post fluid change. Lentivirus-containing supernatant was collected, filtered with a 0.45 μm filter membrane, and stored at -80°C. HEK-293T, HepG2 cells, and A549 cells were infected with lentivirus and selected with puromycin (2 μg/mL) to obtain stable expressing target cells.

Generation and purification of sEVs.

Cells and genetically engineered cells were grown in 15 mm culture dishes and allowed to proliferate. When cells reached 80% confluence, the culture medium was replaced with a similar volume of DMEM supplemented with 0.5% exosome-free FBS [the supernatants were centrifuged at 100,000 × g for 12 h (Beckman Coulter, Optima L-100XP) using normal FBS]. After incubating for 36–48 h, exosomes were extracted using traditional gradient centrifugation methods. To prevent exosome degradation, all centrifugation steps were performed at 4 °C. In brief, culture supernatants were centrifuged at 500 × g for 10 min, 2000 × g for 20 min and 10,000 × g for 40 min successively to remove dead cells, cell debris and other cell secretions (Beckman Coulter, Allegra X-30R). The supernatants were then centrifuged at 100,000 × g for 90 min (Beckman Coulter, Optima L-100XP) to obtain the exosomes. The pelleted exosomes were resuspended in 50–150 μL precooled PBS and stored at -80 °C immediately for the

following experiments. It should be noted that in general, pellets were suspended in RIPA lysis buffer (Thermo Scientific) only for western blot.

Extraction and culture of umbilical cord mesenchymal stem cells (UC-MSCs).

Fresh umbilical cord of approximately 10 cm was obtained after cesarean section, the remaining blood of the umbilical cord was washed thoroughly with normal saline, and then cut into small segments of 2–3 cm, and then rinsed again. The umbilical cord was cut vertically, then one umbilical vein and two umbilical arteries were removed, and Huatong glue was extracted. Ophthalmic scissors were used to cut the Huatong glue into small tissue blocks of 1 mm, which were then transferred to cell culture bottles. DMEM/F12 was added to culture medium containing 10% FBS, 1× penicillin/streptomycin, then cultured in an incubator with 5% CO_2 and at 37°C for static cultures. Cell growth was observed under an inverted microscope every day. The liquid was changed for the first time after 1 week, and once every 3–4 days thereafter. When the cells were 80% ~ 90% long, trypsin/EDTA digestion solution was used for digestion and passage.

Western blot.

Cell lysates and exosomes including purified membrane vesicles were separated by SDS-PAGE and were then transferred to polyvinylidence fluoride membranes (Millipore, Darmstadt, Germany). The membrane was sealed with 5% non-fat milk for more than 1 h at room temperature and incubated with the desired primary antibodies overnight at 4 ℃. Post incubation with HRP-conjugated secondary antibodies was performed for 1 h at room temperature, then detection was carried out using enhanced chemiluminescence reagent (ECL) (Protein Tech, China).

Characterization of sEVs.

The size and zeta potential of exosomes in PBS were determined using a NanoBrook 90Plus PALS (Brookhaven instruments). Data recorded are the average of three measurements. A transmission electron microscopy (TEM, hc-1, Hitachi) at 80 kV was used to observe the morphology of the exosomes. 10 μL of purified exosomes were suspended in PBS and placed

on formvar-carbon-coated copper grids. After 10 min, the residual liquid was removed from the grid edge with filter paper. Exosomes on the grids were then stained with 2% uranyl acetate for 10 min, washed with deionized water 3 times, each time for 10 min, then air-dried.

sEVs cell binding assay.

For HEK-293T-LAG-3-OFP and HEK-293T-PD-1-GFP cells, cells were seeded respectively in confocal dishes, incubated with FP sEVs for 30 minutes the next day, then membranes were stained with WGA 350 for 15 min and observed with a confocal microscope. Jurkat cells were pre-stained with WGA 350 for 15 min and incubated with FP sEVs for 30 min, then spun onto glass slides and observed by confocal microscopy (Zeiss, LSM880).

FK506 loading.

The mixtures containing 200 μg FK506 and 1 mg sEVs diluted in PBS were added to 0.4 cm electroporation cuvettes and were subjected to electroporation at 300 V and 150 μF using a Bio-Rad Gene Pulser Xcell Electroporation System. For membrane recovery, samples in electroporation cuvettes were incubated on ice for 30 min and rinsed gently with PBS to gain suspension. Following centrifugation at 12,000 × g for 10 min, the resulting pellets were washed with cold PBS 3 times and resuspended in PBS for further application.

Isolation of PBMC and T cells from human peripheral blood.

Peripheral blood from normal healthy donors was collected into EDTA potassium vacuoles. PBMCs were isolated using Ficoll lymphocyte isolation medium. Next, $CD3^+$ T lymphocytes were purified (> 98%) by negative selection with MojoSort^{TM} Human $CD3^+$ T cell Isolation Kit (Biolegend, USA). Cells were seeded in CD3-coated plates (clone OKT3; Biolegend) and cultured in medium (RPMI1640 with 10% FBS, penicillin/streptomycin, and 2 ng/mL IL-2).

CFSE staining.

A CFSE separation and tracking kit (Biolegend, USA) was used to label PBMCs as a CFSE working solution (5 μM). T cells were incubated at 37 °C for 20 min, and then quenched and stained with culture medium on 0, 3, 5, and 7 days respectively. Cells were collected and

subjected to FACS (Cytoflex, Beckman, USA) using the Cell Quest software (CytExpert, USA).

Biological distribution of sEVs.

Cy5.5-labeled sEVs, Free sEVs and FP sEVs were injected into BALB/c mice as a 200 μL (2 μg/μL) solution via the tail vein. After 2 h, accumulation of sEVs in various organs was observed using a NightOWLimaging system (LB983).

Mouse heart graft model.

The use of laboratory animals and all animal experiments was reviewed and approved by the Animal Ethics Committee of the Zhongshan School of Medicine, Sun Yat-sen University, China. The approval number is SYSU-IACUC-2019-000332. Heart transplantations were carried out using male BALB/c mice as donors. Hearts were transplanted into the necks of male C57BL/6 mice (8-10 weeks old, weight >22 g). The doses and injection time of all 78 recipients were randomly divided into four equal groups: group 1 (negative control group, n = 8), group2 (injected with saline, n = 10), group 3 (Free sEVs 25 mg/kg/d, n = 10), group 4 (FGL1 sEVs 25 mg/kg/d, n = 10), group 5 (PD-L1 sEVs 25 mg/kg/d, n = 10), group 6 (FK506 1.0 mg/kg/d, n = 10), group 7 (FGL1/PD-L1 sEVs 25 mg/kg/d, n = 10), and group 8 (FGL1/PD-L1 sEVs@FK506 25 mg/kg/d, n = 10). The recipients were treated via tail vein injection every day, until 30 days after transplantation. Transplanted mice were then sacrificed at 7 days to dissect grafted-hearts, lymph nodes, and spleens, which were subjected to downstream analysis.

Histology and immunohistochemistry analysis.

Seven days after heart graft surgery, the mouse recipients were sacrificed and tissue examples from the transplantation location were collected in 15 mL centrifugal tubes, and the entirety of samples were submerged with 4% paraformaldehyde for fixation. Next, the samples were embedded with paraffin and were sectioned (4 μm thickness). Sections were stained with hematoxylin and eosin (H&E) using standard procedures. Inflammatory cell infiltration conditions were observed by fluorescence microscopy with 4x, 10x, 20x and 40x magnification. For the immunohistochemical staining, deparaffinized tissue sections were incubated with mouse monoclonal CD3 (PC3/188A: sc-20047, Santa Cruz Biotechnology), followed by

visualization using an HRP/DAB detection IHC Kit. Sections were counterstained with Mayer's hematoxylin. The infiltrated parts of lymphocytes were also photographed as above.

RNA isolation and qPCR analysis.

The total RNA was collected and purified from cells or spleen tissue using TRIZOL reagent (TaKaRa, Tokyo, Japan) according to the manufacturer's protocol. RNA concentrations were measured using NANODROP ONE (Thermo Fisher Scientific). RNA was reversely transcribed into complementary DNA (cDNA) using HiScript III RT SuperMix for qPCR (+gDNA wiper) (TransGen Biotech, China) with a PCR Instrument (BIO-RAD), and then quantified by qPCR using 2x SYBR Green qPCR Mix (TransGen Biotech, China) with LightCycler® 96 (Roche). Relative gene expression folding changes were identified with the $2^{-\Delta\Delta Ct}$ method. The qPCR primers for all the experiments are listed in Supplementary Table 2.

RNA Sequencing.

RNA extraction and qualification: PBMCs were extracted from healthy volunteers. sEVs from different treatment groups were co-incubated with PBMCs for 48 h, then RNA was extracted using TRIZOL reagent (TaKaRa, Tokyo, Japan). RNA degradation and contamination were monitored on 1% agarose gels. RNA purity and concentration were checked using a NanoPhotometer® spectrophotometer (IMPLEN, CA, USA) and Qubit® RNA Assay Kit in Qubit® 2.0 Flurometer (Life Technologies, CA, USA). RNA integrity was assessed using an RNA Nano 6000 Assay Kit from the Bioanalyzer 2100 system (Agilent Technologies, CA, USA). The RNA-seq library was then generated using the NEBNext® Ultra™ RNA Library Prep Kit for Illumina® (NEB, USA). Library quality was assessed using the Agilent Bioanalyzer 2100 system. Subsequent sequencing was performed using an Illumina Novaseq System (Illumina, USA). Library construction and sequencing were carried out at Berry Genomics. For data analysis, differential expression analysis of two conditions was performed using the DEGSeq R package. The *P* values were adjusted using the Benjamini & Hochberg method. A corrected *P* value of 0.05 and log 2 (fold change) of 1 were set as the threshold for significantly differential expression.

MiRNA Sequencing.

RNA from EVs was extracted using an RNA miRNeasy Micro Kit (Qiagen, Germany). RNA quantity and purity were determined by a Nanodrop (Thermo Fisher Scientific Inc., USA) and an Agilent 4200 Tape station (Agilent, CA, USA). Library construction for the paired-end libraries was performed using a QIAseq miRNA library kit (Qaigen, Germany). Subsequent sequencing was performed on the Illumina Novaseq System (Illumina, USA). Library construction and sequencing were carried out at Shanghai Biochip Corporation. For data analysis, the reading of each miRNA-seq sample was compared with the existing sequence in the miRBase and the predicted result of the new miRNA in order to calculate the expression level count (counts per million) of the miRNA. The edgeR software package was used to analyze the expression between samples and screen out UMI counts with a *P* value of <0.05 and a fold change of >2.0.

Flow cytometric analysis.

Seven days after heart transplantation, the superficial cervical lymph nodes on the surgical side, graft-heart, and spleens of the mice were dissected and placed in 1.5 mL EP tubes. The hearts were cut with scissors, and the spleens and lymph nodes were ground with a mortar. A single cell suspension was obtained by passing the suspension through a 70-mesh cell sieve. The cells were centrifuged at 1500 × g for 5 min at 4 °C, then resuspended and centrifuged twice with RBC lysis buffer to obtain cell pellets. These mononuclear cell suspensions were labeled with FITC-CD3, APC-conjugated CD4, BV510-conjugated CD8, PE-conjugated CD25 and Pacific Blue -conjugated Foxp3 monoclonal antibodies, then subjected to FACS (Cytoflex, Beckman, USA) using the Cell Quest software (CytExpert, USA).

Statistical Analysis.

Three independent sample replicates were carried out for each experiment unless stated otherwise. The statistical significance between the two groups was measured using the unpaired Student's t-test. All results are expressed as the mean ± SD. Data analysis and processing was done using GraphPad Prism Ver 8.0 (GraphPad Software). One-way analysis of variance (ANOVA) or Student's t-test was performed, and statistical significance was indicated (*, $p <$

0.05; **, $p < 0.01$; ***, $p < 0.001$).

Results

LAG-3/PD-1 is inconsistent with FGL1/PD-L1 in organ transplant recipients with rejection.

In order to demonstrate if activating inhibitory axes could be advantageous for the relief of immunologic rejection, we first checked mRNA expression levels among a panel of immune checkpoint genes in a heterotopic heart allograft mouse model. We found that among these checkpoint genes, LAG-3 and PD-1 mRNA in the spleens were simultaneously upregulated 8.56- and 6.24 fold higher in the transplantation group (**Figure 1A**). We then further checked LAG-3 and PD-1 expression in peripheral blood mononuclear cells (PBMCs) of clinical renal transplant patients. We found that LAG-3 and PD-1 expression in T cell-mediated rejection (TCMR) patients was significantly higher than both in antibody-mediated rejection (ABMR) recipients and non-rejection recipients after kidney transplantation (**Figures 1B-C**). We therefore speculated that the up-regulated expression of LAG-3 and PD-1 following the occurrence of organ transplant rejection is a key step in the initiation of T cell immunological tolerance. Surprisingly, neither PD-1 ligand PD-L1 nor the newly discovered inhibitory ligand of LAG-3, FGL1 increased in the spleens of transplanted mice. (**Figure 1D**). Thus, we speculated that the simultaneous enhancement of FGL1 and PD-L1 inhibitory molecules would be a potential strategy to activate the PD-L1/PD-1 and FGL1/LAG-3 inhibitory axes, thereby inhibiting $CD8^+$ T cell activation and reestablishing immune tolerance of the graft.

Establishment and Characterization of FGL1/PD-L1 Dual-Targeting sEVs. Recently, small extracellular vesicles (sEVs) released by metastatic melanomas carrying PD-L1 on their surface were reported to successfully suppress the function of $CD8^+$ T cells [36], which provided us with a rationale for developing FGL1 and PD-L1 dual-targeting sEVs as an anti-rejection therapy. As the expression of FGL1 and PD-L1 in HEK-293T, HepG2, A549, and MSC cell lines were inconsistent (**Figure 2A**), simultaneous high expression of both FGL1 and PD-L1 on sEVs from the same natural cell line would be difficult. Furthermore, FGL1 and PD-L1 expression in purified sEVs were low and fluctuated between four different cell lines

(**Figure 2B**). Thus we speculated that bioengineering sEVs that co-expressed both FGL1 and PD-L1 to a relatively high degree may serve as a strategy to relieve T-cell mediated graft rejection. As FGL1 is a soluble protein and may not be expressed on the membrane of sEVs, we first reconstructed a membrane-localized form of FGL1 vector (FGL1-TM) by fusing a transmembrane sequence [37]. Next, FGL1-TM vector were transferred together with PD-L1 vector by lentiviral transfection into HEK-293T, HepG2, A549, and MSC to establish stable cell lines overexpressing FGL1/PD-L1 (**Figure 2C**). Western blotting analysis (**Figure 2D**) and confocal images (**Figure 2E**) cooperatively confirmed FGL1 and PD-L1 were co-expressed and localized on the cell membrane.

Next, we prepared and purified dual-targeting FGL1/PD-L1 sEVs (FP sEVs) derived from HEK-293T-FP, HepG2-FP, A549-FP and MSC-FP cells by differential centrifugation to test if overexpressing FGL1 and PD-L1 induced the enrichment of FGL1 and PD-L1 on sEVs. Western blotting confirmed the co-existence of exogenous FGL1 and PD-L1 in the sEVs derived from HEK-293T, HepG2, A549, and MSC cell lines, indicated by the exosomal markers CD63, CD9, and Alix in isolated vesicles, which were much higher in sEVs derived from bioengineering cells (FP sEVs) than unmodified cells (sEVs) (**Figure 3A**). Interestingly, MSC-FP sEVs expressed much more FGL1/PD-L1 than FP sEVs derived from other cell lines. The transmission electron microscopy (TEM) images showed that sEVs derived from different cell lines were round-shaped and membrane bound (**Figure 3B**). Dynamic light scattering (DLS) analysis further verified similar size and stability of all types of sEVs, with the average diameter of 110 nm and an average zeta potential of -30 mV (**Figures 3 C-D**).

As miRNAs derived from MSC sEVs are reported to maintain and regulate immune function [38, 39], we performed miRNA sequencing on HEK-293T and MSC derived sEVs to verify if miRNAs from MSC sEVs have significant immunomodulatory potential. Using 4,872 Immunologic Signature Gene Sets provided by the GSEA website, miRNAs targeting these immune genes were mined from the original sequencing data and presented in the form of heat map (**Figure S1A**). An extensive literature survey revealed that 9 out of top 20 up-regulated and 2 out of top 20 down-regulated miRNAs have been proven to play a role in negative

immune regulation (**Table S2**), of which we further validated three top-scored upgraded miRNAs (miR-125b-5p, let-7b-5p, and miR-21-5p) in MSC sEVs than HEK-293T sEVs by quantitative real-time PCR**(Figure S1B)**. In line with sequencing results, MSC sEVs showed a stronger inhibition on PBMCs and T cells proliferation than HEK-293T sEVs through an *in vitro* CFSE cell proliferation assay (**Figure S1C**). All these data suggest that MSCs are the optimal choice for bioengineering dual-targeting FGL1/PD-L1 sEVs due to abundant expression of target proteins and potent immune regulation capacity. Confocal microscopy further verified the co-presence of FGL1-GFP and PD-L1-OFP on the membrane of sEVs derived from MSCs (**Figure 3E**). Similar to MSC sEVs, MSC-FP sEVs also contains the same nine upregulated and two downregulated miRNAs of negative immunoregulation function when compared with HEK-293T sEVs (**Figure S2 and Table S2**), indicating that our genetic modification does not affect major immune modulatory miRNA signature in sEVs. In addition, we constructed MSC cell lines overexpressing single target FGL1 or PD-L1 and GFP/OFP vector (**Figure S3**), single-targeting PD-L1 and FGL1 sEVs were also prepared from MSCs and subjected to DLS analysis. There were no statistically significant differences in size, distribution pattern, and zeta potentials between single target sEVs and dual-targeting FGL1/PD-L1 sEVs (FP sEVs) (**Figure S4**).

FGL1/PD-L1 sEVs inhibited T cell proliferation through the interaction of FGL1/LAG-3 and PD-L1/PD-1 *in vitro*.

To investigate whether FGL1 or PD-L1 sEVs were able to effectively bind to their target molecules, we conducted the following experiments. First, PD-L1 or FGL1 sEVs were respectively incubated with OFP-LAG-3- and GFP-PD-1-expressing HEK-293T cells. Confocal images revealed a distinct colorization of FGL1-GFP/LAG-3-OFP and PD-L1-OFP/PD-1-GFP on the membranes of HEK-293T (**Figure 4A**). As known, FGL1/LAG3 and PD-L1/PD-1 were two immunonegative regulatory pathways that played a major role in inhibiting T cell activation, so it was necessary to explore whether modified dual-targeting FGL1/PD-L1 sEVs (FP sEVs) could interact with LAG3/PD-1 expressing T cells. Consistent with the result of heart transplant model (**Figure 1A**), the mRNA levels showed that LAG-3 and PD-1 expression had increased when Jurkat cells were simulated by PMA/ Ionomycin (PI)

(**Figure S5**). FP sEVs were incubated with PI-stimulated Jurkat T cells consequentely. Confocal microscopy revealed a distinct co-localization of FP sEVs on the surface of activated Jurkat cells (**Figure 4B**). This indicates that FGL1/PD-L1 sEVs could bind specifically to LAG-3/PD-1 receptors.

As overactive T cells are negatively regulated through the co-inhibitory pathway comprising FGL1/LAG-3 and PD-L1/PD-1, we explored the functional role of FP sEVs on the inhibition of T cell activation. First, healthy human PBMCs were extracted and co-incubated with Free sEVs (from control vector infected MSC), FGL1 sEVs, PD-L1 sEVs, and FP sEVs respectively. The mRNA resulting from each treatment was extracted and subjected to RNA-seq analysis after 48 h. It was immediately apparent that the concentration and number of regulatory cytokines were different between single target FGL1 or PD-L1 sEVs, and double target FP sEVs as compared to Free sEVs. However, FP sEVs had 9 and 14 overlapping cytokines as compared to the FGL1 sEVs and PD-L1 sEVs treatment groups respectively. In addition, the specific changes of 34 cytokines in the FP sEVs treatment group may be the reason for stronger efficacy observed than that of any single target treatment group (**Figure 4C**). Further analysis of these altered genes revealed that FGL1 sEVs decreased *IL-2*, *IL-22*, and *IL-18*, and increased *IL-10* as compared with the Free sEVs group (**Figure 4D)**. *IL-5*, *IL-17A*, *IL-17F*, and *IL-21* decreased in PD-L1 sEVs compared with Free sEVs (**Figure 4E)**. In comparison to the Free sEVs group, the changes of cytokines in the FP sEVs group were more prominent (**Figure 4F)**. In conclusion, the co-expression of the FGL1/PD-L1 can affect the proliferation and differentiation of immune cells to some extent by affecting more immune cytokines.

In addition to RNA-sequencing, we also detected the mRNA levels of specific transcription factors in Th1, Th2, Th17, and Treg cells (**Figure 4G**). We found that *TBET* and *RORγt* transcription factors were down-regulated, indicating that our dual-targeting sEVs were able to suppress the differentiation of Th1 and Th17, thus inhibiting the function of T cell proliferation and differentiation. They also affected a concomitant increase in *FOXP3*, indicating an ability to increase the proportion of Treg cells. The sEVs were also able to increase the expression of *GATA3*, which is suggestive of a promotion in Th2 differentiation. According to previous

reports, down-regulation of the Th1/Th2 ratio promotes stability of the immune environment after organ transplantation.

In order to clarify how our artificially modified sEVs affected downstream signaling in the T cell receptor (TCR) pathway, Jurkat cells were lysed in order to observe related proteins after 48 h incubation with different sEVs groups. PD-1/LAG3 involved in TCR pathway is clearly described in the **Figure 4H**, the results showed that p-LCK, p-AKT (Thr308), p-ZAP70 were down-regulated, thus inhibiting T cell proliferation and activation. SHP2 is a signaling protein recruited by the synergistic action of LAG-3 and PD-1. Its role is to inhibit rapid protein phosphorylation occurring at T cell downstream signaling sites, thereby weakening T cell function (**Figure 4I**). Additionally, FP sEVs showed a stronger effect on elevating SHP2 while reducing p-LCK and p-AKT (Thr308) expression compared with FGL1 sEVs or PD-L1 sEVs. Therefore, the modified sEVs could inhibite T cell proliferation and T cell function via suppressing immune cytokines, T cell differentiation, and TCR downstream pathway proteins.

Lastly, CFSE-labeled $CD3^+$ T cells were cultured with Free sEVs, FGL1 sEVs, PD-L1 sEVs, and FP sEVs respectively for 7 days. The following flow cytometry analysis showed that FGL1, PD-L1, and FP sEVs significantly inhibited the proliferation of $CD3^+$ T cells by 11.6%, 7.08%, and 17.58% respectively, suggesting that FP sEVs had a stronger immunosuppressive effect than that of FGL1 or PD-L1 single-targeted sEVs (**Figure 4J**). This was supported by corresponding quantitative analysis of CFSE results (**Figure 4K**).

FK506 is the most widely used immunosuppressive agent in tissue and organ transplantation rejection, and acts by preventing Ca^{2+}-calcineurin-NFAT signaling, the master regulator of T cell proliferation and activation [35, 40]. To investigate the efficacy of FGL1/PD-L1 sEVs as a synergistic, targeted drug delivery system of FK506 to effector T cells, we prepared coated vesicles (FP sEVs@FK506) using an electric transformer. The average drug loading percentage was 23.58% (**Figure S6**). As compared to FK506 and FP sEVs administered alone, FP sEVs@FK506 achieved the highest inhibition rate of 69.92% on T cell proliferation (**Figure 4J-K)**, suggesting that, FP sEVs@FK506 greatly enhanced the inhibition function of FK506.

FGL1/PD-L1 sEVs prolonged graft survival time and induced immune tolerance in a heart graft model.

The immunosuppressive effects of FP sEVs in a heart graft model were further evaluated. We first infected mouse FGL1/PD-L1 on MSC cells to obtain stable cell lines (**Figure S7**), and then extracted enough sEVs for drug administration to further assess whether FP sEVs showed better inhibitory effect in transplant rejection. In addition, we performed verification experiments in a mouse cardiac allograft model, an excellent tool to study immunological mechanism[41]. The hearts of BALB/c mice were transplanted to the cervices of C57BL/6 mice. The recipient mice were then grouped into seven clusters containing saline, Free sEVs, PD-L1 sEVs, FGL1 sEVs, FP sEVs, FK506, and FP sEVs@FK506 (**Figure 5A**). Bioluminescent images of FP sEVs taken *in vivo* confirmed a marked increase in accumulation on cervical graft-heart sites as compared to both sEVs (from natural MSCs) and Free sEVs (from control vector infected MSCs) (**Figure S8A**). There was no difference significant in body weight change between each groups. (**Figure 5B**). Simultaneously, toxicological experiments were also performed, including a histopathological assay and blood cell counts, which proved that our sEVs did not produce other obvious side effects elsewhere in the mice (**Figure S8B-C)**. Among these groups, FP sEVs showed notably prolonged heart-graft survival (Figure 5C) and a declining trend of $CD8^+$ T cells was observed in spleens and grafted hearts (Figure 5D-E). In contrast to this, $CD4^+$ $CD25^+$ $Foxp3^+$ regulatory T cells (Treg cells) were more prevalent in the superficial cervical lymph nodes of heart-transplanted mice that injected with FP sEVs (Figure 5F). Similarly, FP sEVs could cooperate with FK506 (FP sEVs@FK506) showed the greatest propensity to reduce the number of $CD8^+$ T cells in spleens and transplanted hearts (Figure 5D-E), and increase $CD4^+CD25^+Foxp3^+$ Treg cells. (**Figure 5F**)**.** Remarkably, FP sEVs and FP sEVs@FK506 precluded immune rejection via decreasing levels of inflammatory cells and infiltrated $CD3^+$ T cells (**Figure 5G**). We further detected mRNA levels of *Granzyme B* and *Il-12* in recipient spleens, as the presence of cytokines is also reflective of the activation capacity of immune cells. FGL1 sEVs, PD-L1 sEVs, FP sEVs, and FP sEVs@FK506 treatment groups displayed a prominent reduction of *Granzyme B* and *Il-12* mRNA levels (**Figure 5H**). Furthermore, ELISA results also showed that all sEVs treatment groups exhibited a significant reduction of TNF-α

and noticeable rise of TGF-β1, especially in the FP sEVs and FP sEVs@FK506 sEVs group, compared to the saline or Free sEVs groups **(Figure 5I)**. Overall, this supports the conclusion that FP sEVs exhibit a synergistic immunosuppressive function with FK506 to prevent graft rejection and reestablish immune tolerance.

Discussion

As a summary, we established a designed MSCs-derived dual-targeting FGL1/PD-L1 sEVs for inhibiting immunological rejection. This dual-targeting drug delivery system also demonstrate the stronger power to carry low dose of FK506 to LAG-3/PD-1 expressing effector T cells, thus inhibiting T cell activation and proliferation, and induce Tregs in organ recipient mice. Our study provides an experimental basis for a novel intervention strategy that leverages functions of target delivery sEVs to synergistically enhance two immunosuppression axes and reestablish immune tolerance, ultimately, promoting organ acceptance (**Figure 6**).

LAG-3 is reported to be synergistic with PD-1 inhibitory effect on T cell signaling during cancer immune escape [42]. Dual antibody blockade or genetic knockout of LAG-3 and PD-1 significantly enhanced T effector function and delayed tumor growth. In this study, LAG-3 and PD-1 were detected simultaneously up-regulated expression under an organ transplant rejection environment so as to maintain immune tolerance, providing a solid foundation for the concurrent construction of double-targeting immunosuppressant. Membrane-based nanovesicles including erythrocytes, platelets, or nanovesicles obtained by the grinding and centrifugation of cell membranes have enormous potential to behave as drug delivery vehicles owing to their small size and biocompatibility [43-45] [46, 47]. However, there are a number of problems associated with their preparation, including membrane incompleteness, turnover of inner and outer membranes, especially

high immunogenicity. As a natural membrane delivery system, sEVs present themselves as an excellent alternative biological vector. However, whether two ligand proteins can be simultaneously highly expressed on the membrane of sEVs by genetic engineering has not been reported before. Herein, we presented the first report on immune checkpoints dual-targeting

sEVs and their application in organ transplantation. Furthermore, we determined that MSCs-derived sEVs prior to that from other cell sources can inherit the properties of immune modulation and tolerance of MSCs itself, and will be therefore a promising biomaterial for immunotherapies.

We modified sEVs to simultaneously carry two targets exogenously, but it is unclear whether such a manipulation affects sEVs quality and function. Indeed, the difficulty in controlling the quality and function of modified sEVs remains a substantial obstacle in their development as a novel therapeutic strategy. We therefore compared sEVs from a diverse range of cell sources and also analyzed the contents of engineered sEVs, which led to the conclusion that the variation in sEVs contents should be closely monitored in order to ensure a high level of quality control during the modification process.

Tregs play an important role in establishing immune tolerance, preventing excessive immune response and eliminating autoimmunity. Tregs has been widely studied as a cell therapy in the treatment of GvHD and limiting graft rejection. However, previous studies have reported that Foxp3 in Treg cells are less NFAT-independent, so two of the most commonly used immunosuppressants of FK506 and Cyclosporin A, the inhibitors of NFAT signaling pathway, can not effectively reconstruct Treg cell subsets in patients with organ transplantation rejection[35, 48, 49]. Excitedly, we found that FP sEVs@FK506 have additional function to induce regulatory T cells in the recipient surgical lymph nodes, indicating the power of combining low-dose FK506 with FGL1/PD-L1 on sEVs as immunosuppressants to promote allograft acceptance. This underscores the remarkable function of immune checkpoints in excessive immunity. In the future, bioengineering sEVs carrying multiple disease-mediating receptors or cross-talking signaling cascades may become a common therapeutic strategy.

Disclosure of interest

The authors report no conflict of interest.

Acknowledgements

This research was supported by the National Natural Science Foundation of China (81702750, 81970145 and 82001698); Natural Science Foundation of Guangdong Province (2020A1515011465 and 2020A151501467); Science, Technology & Innovation Commission of Shenzhen Municipality (JCYJ20170818164756460, JCYJ20180307154700308, JCYJ20170818163844015, JCYJ20180307151420045 and JCYJ20190807151609464); Sun Yat-sen University (20ykzd17 and 20ykpy122); International Collaboration of Science and Technology of Guangdong Province (2020A0505100031).

References

[1] Dumont F. FK506, an immunosuppressant targeting calcineurin function. Curr Med Chem. 2000; 7(7)**:** 731-748.

[2] Vincenti F, Jensik SC, et al. A long-term comparison of tacrolimus (FK506) and cyclosporine in kidney transplantation: evidence for improved allograft survival at five years1. Transplantation. 2002; 73(5)**:** 775-782.

[3] Group USMFLS. A comparison of tacrolimus (FK 506) and cyclosporine for immunosuppression in liver transplantation. N Engl J Med. 1994; 331(17)**:** 1110-1115.

[4] Lee J-U, Kim L-K, et al. Revisiting the concept of targeting NFAT to control T cell immunity and autoimmune diseases. Front immunol. 2018; 9**:** 2747.

[5] Lechler RI, Sykes M, et al. Organ transplantation—how much of the promise has been realized? Nat Med. 2005; 11(6)**:** 605-613.

[6] Cahalan MD. Imaging transplant rejection: a new view. NAT MED. 2011; 17(6)**:** 662-663.

[7] Cheung CY, Tang SCW. An update on cancer after kidney transplantation. Nephrol Dial Transplant. 2019; 34(6)**:** 914-920.

[8] Gioco R, Corona D, et al. Gastrointestinal complications after kidney transplantation. World J Gastroenterol. 2020; 26(38)**:** 5797-5811.

[9] Long L, Zhang X, et al. The promising immune checkpoint LAG-3: from tumor microenvironment to cancer immunotherapy. Genes. 2018; 9(5-6)**:** 176-189.

[10] ElTanbouly MA, Zhao Y, et al. VISTA is a checkpoint regulator for naïve T cell quiescence and peripheral tolerance. Science. 2020; 367(6475)**:** 1-14.

[11] Tu L, Guan R, et al. Assessment of the expression of the immune checkpoint molecules PD-1, CTLA4, TIM-3 and LAG-3 across different cancers in relation to treatment response, tumor-infiltrating immune cells and survival. Int J Cancer. 2020; 147(2)**:** 423-439.

[12] Assal A, Kaner J, et al. Emerging targets in cancer immunotherapy: beyond CTLA-4 and PD-1. Immunotherapy. 2015; 7(11)**:** 1169-1186.

[13] Yin Z, Yu M, et al. Mechanisms underlying low-clinical responses to PD-1/PD-L1 blocking antibodies in immunotherapy of cancer: a key role of exosomal PD-L1. J Immunother Cancer. 2021; 9(1)**:** e001698.

[14] Ott PA, Hodi FS, et al. CTLA-4 and PD-1/PD-L1 blockade: new immunotherapeutic modalities with durable clinical benefit in melanoma patients. Clin Cancer Res. 2013; 19(19)**:** 5300-5309.

[15] Alsaab HO, Sau S, et al. PD-1 and PD-L1 checkpoint signaling inhibition for cancer immunotherapy: mechanism, combinations, and clinical outcome. Front Pharmacol. 2017; 8**:** 561.

[16] Jiang Y, Zhao X, et al. Progress and challenges in precise treatment of tumors with PD-1/PD-L1 blockade. Front Immunol. 2020; 11**:** 339.

[17] Zhai Y, Moosavi R, et al. Immune Checkpoints, a Novel Class of Therapeutic Targets for Autoimmune Diseases. Front Immunol. 2021; 12**:** 645699.

[18] Wang H, Liu Y, et al. Cell membrane biomimetic nanoparticles for inflammation and cancer targeting in drug delivery. Biomaterials science. 2020; 8(2)**:** 552-568.

[19] Robbins PD, Dorronsoro A, et al. Regulation of chronic inflammatory and immune processes by extracellular vesicles. J Clin Investig. 2016; 126(4)**:** 1173-1180.

[20] Xu Z, Tsai H-i, et al. Engineering programmed death ligand-1/cytotoxic T-lymphocyte-associated antigen-4 dual-targeting nanovesicles for immunosuppressive therapy in transplantation. ACS nano. 2020; 14(7)**:** 7959-7969.

[21] Abril-Rodriguez G, Ribas A. SnapShot: Immune Checkpoint Inhibitors. Cancer Cell. 2017; 31(6)**:** 848-848 e841.

[22] Haanen JB, Robert C. Immune Checkpoint Inhibitors. Prog Tumor Res. 2015; 42**:** 55-66.

[23] Wang X, Zhang H, et al. Cell-derived exosomes as promising carriers for drug delivery and targeted therapy. Curr Cancer Drug Tar. 2018; 18(4)**:** 347-354.

[24] Bunggulawa EJ, Wang W, et al. Recent advancements in the use of exosomes as drug delivery systems. J Nanobiotechnology. 2018; 16(1)**:** 1-13.

[25] Yamamoto T, Kosaka N, et al. Latest advances in extracellular vesicles: From bench to bedside. Sci Technol Adv Mat. 2019; 20(1)**:** 746-757.

[26] Meldolesi J. Exosomes and ectosomes in intercellular communication. Curr Biol. 2018; 28(8)**:** R435-R444.

[27] Chen G, Huang AC, et al. Exosomal PD-L1 contributes to immunosuppression and is associated with anti-PD-1 response. Nature. 2018; 560(7718)**:** 382-386.

[28] Ramsay AG. Immune checkpoint blockade immunotherapy to activate anti-tumour T-cell immunity. Brit J Heamatol. 2013; 162(3)**:** 313-325.

[29] Lai P, Weng J, et al. Novel insights into MSC-EVs therapy for immune diseases. Biomark Res. 2019; 7(1)**:** 1-10.

[30] Salem HK, Thiemermann C. Mesenchymal stromal cells: current understanding and clinical status. Stem Cells. 2010; 28(3)**:** 585-596.

[31] Lai P, Chen X, et al. A potent immunomodulatory role of exosomes derived from mesenchymal stromal cells in preventing cGVHD. J Hematol Oncol. 2018; 11(1)**:** 135.

[32] Wang L, Gu Z, et al. Extracellular Vesicles Released from Human Umbilical Cord-Derived Mesenchymal Stromal Cells Prevent Life-Threatening Acute Graft-Versus-Host Disease in a Mouse Model of Allogeneic Hematopoietic Stem Cell Transplantation. Stem Cells Dev. 2016; 25(24)**:** 1874-1883.

[33] Kordelas L, Rebmann V, et al. MSC-derived exosomes: a novel tool to treat therapy-refractory graft-versus-host disease. Leukemia. 2014; 28(4)**:** 970-973.

[34] Farzamfar S, Hasanpour A, et al. Extracellular micro/nanovesicles rescue kidney from ischemia-reperfusion injury. J Cell Physiol. 2019; 234(8)**:** 12290-12300.

[35] Tsai Hi, Zeng X, et al. NF45/NF90-mediated rDNA transcription provides a novel target for immunosuppressant development. EMBO Mol Med. 2021; 13(3)**:** e12834.

[36] Su D, Tsai H-I, et al. Exosomal PD-L1 functions as an immunosuppressant to promote wound healing. J Extracell Vesicles. 2020; 9(1)**:** 1709262.

[37] Wang J, Sanmamed MF, et al. Fibrinogen-like protein 1 is a major immune inhibitory ligand of LAG-3. Cell. 2019; 176(1-2)**:** 334-347.

[38] Lee HK, Finniss S, et al. Mesenchymal stem cells deliver exogenous miRNAs to neural cells and induce their differentiation and glutamate transporter expression. Stem Cells Dev. 2014; 23(23)**:** 2851-2861.

[39] Ti D, Hao H, et al. LPS-preconditioned mesenchymal stromal cells modify macrophage polarization for resolution of chronic inflammation via exosome-shuttled let-7b. J Transl Med. 2015; 13(1)**:** 1-14.

[40] Bentata YJAo. Tacrolimus: 20 years of use in adult kidney transplantation. What we should know about its nephrotoxicity. Artificial organs. 2020; 44(2)**:** 140-152.

[41] Costello R, Kissenpfennig A, et al. Development of transplant immunosuppressive agents - considerations in the use of animal models. Expert Opin Drug Discov. 2018; 13(11)**:** 1041-1053.

[42] Huang R-Y, Eppolito C, et al. LAG3 and PD1 co-inhibitory molecules collaborate to limit CD8+ T cell signaling and dampen antitumor immunity in a murine ovarian cancer model. Oncotarget. 2015; 6(29)**:** 27359.

[43] Żmigrodzka M, Guzera M, et al. The biology of extracellular vesicles with focus on platelet microparticles and their role in cancer development and progression. Tumor Biology. 2016; 37(11)**:** 14391-14401.

[44] Zhang X, Wang C, et al. PD-1 blockade cellular vesicles for cancer immunotherapy. Adv Mater. 2018; 30(22)**:** 1707112.

[45] Zhang X, Wang J, et al. Engineering PD-1-presenting platelets for cancer immunotherapy. Nano letters. 2018; 18(9)**:** 5716-5725.

[46] Tan S, Wu T, et al. Cell or cell membrane-based drug delivery systems. Theranostics. 2015; 5(8)**:** 863-881.

[47] Ghosh S, Girigoswami K, et al. Membrane-encapsulated camouflaged nanomedicines in drug delivery. Nanomedicine. 2019; 14(15)**:** 2067-2082.

[48] Xu G, Wang L, et al. Rapamycin and tacrolimus differentially modulate acute graft-

versus-host disease in rats after liver transplantation. Liver Transpl. 2010; 16(3)**:** 357-363.

[49] Rudensky AY, Gavin M, et al. FOXP3 and NFAT: partners in tolerance. Cell. 2006; 126(2)**:** 253-256.

Figure Legend

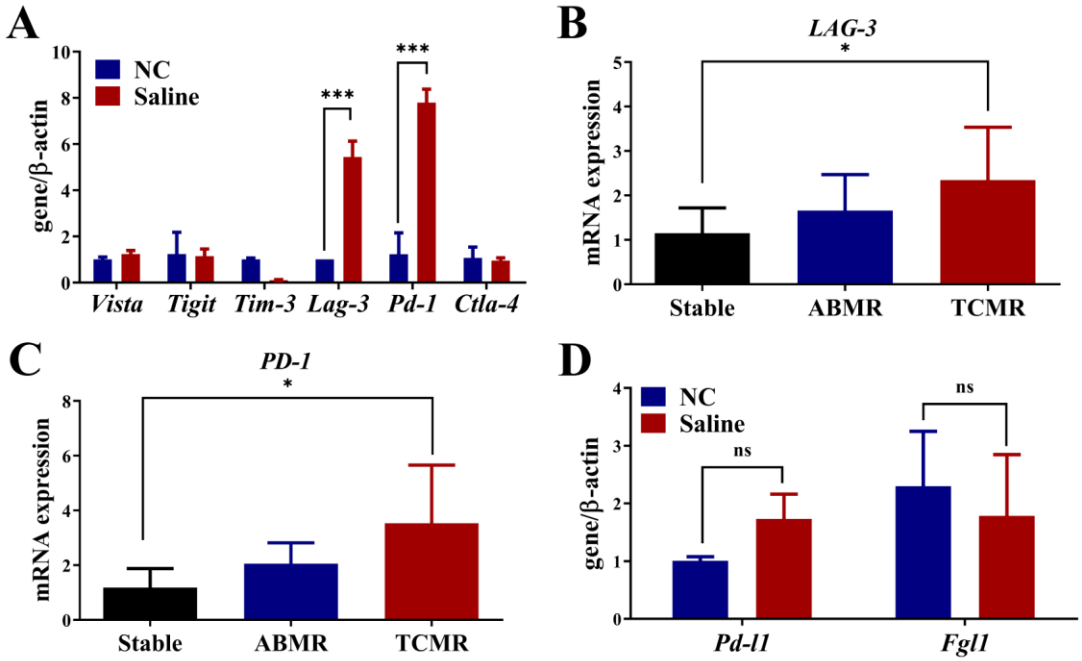

Figure 1. LAG-3/PD-1 is inconsistent with FGL1/PD-L1 in organ transplant recipients with rejection. (A) Quantitative PCR to verify the expression of immune checkpoint receptors in the spleens of heart-graft models, $n = 3$. (B-C) Quantitative PCR to verify the expression of LAG-3 (B) and PD-1 (C) in PBMCs of clinical renal transplant patients, n = 6-7. (D) Quantitative PCR verified the ligand expressions of FGL1 and PD-L1 in the spleens of mouse heart transplant models, $n = 5$. Error bar, mean ± SD. NS: no significant, $*P < 0.05$, $**P < 0.01$, $***P < 0.001$

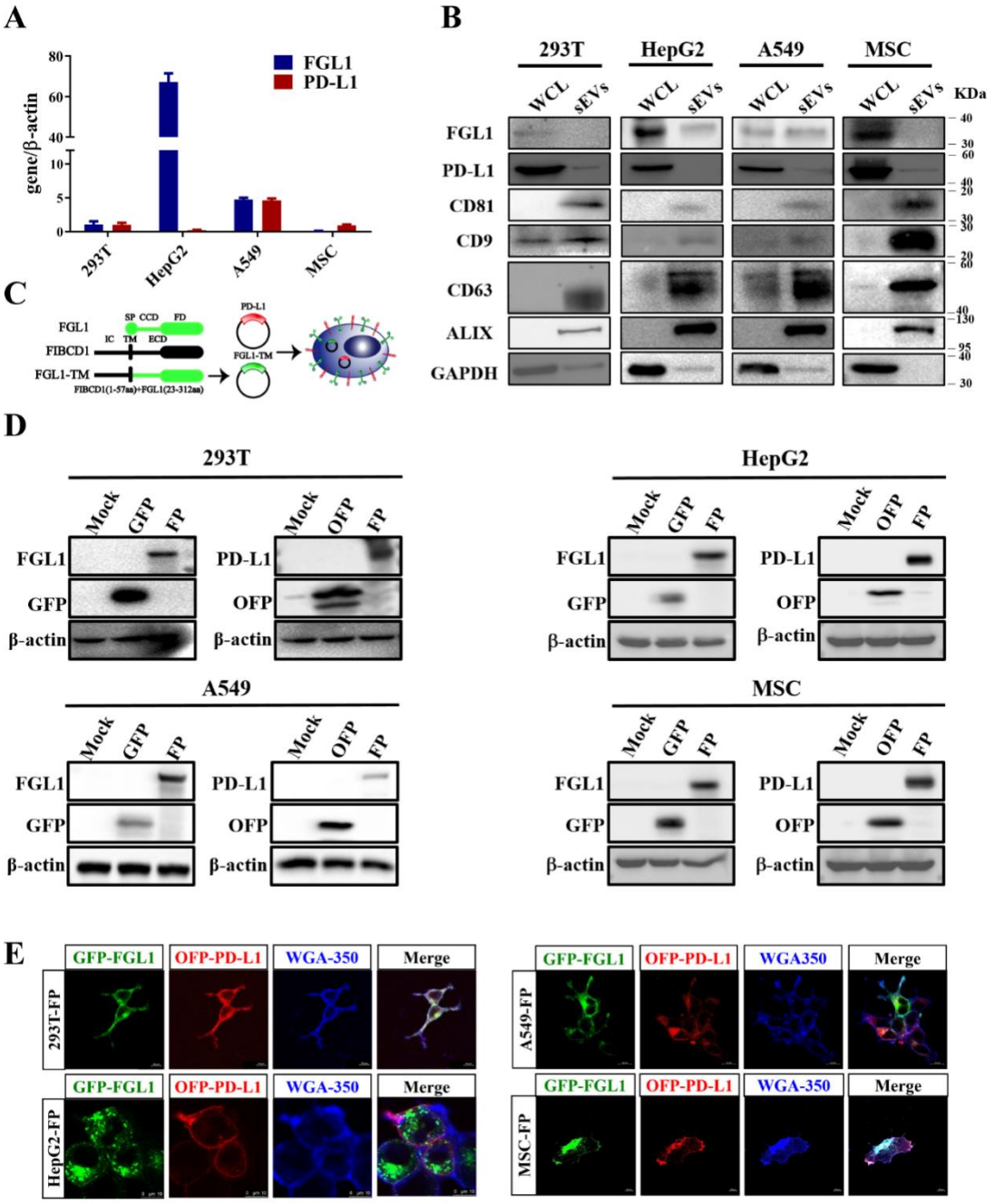

Figure 2. The deficiency of natural exosomes to express FGL1/PD-L1 simultaneously determines the necessity of artificial exogenous overexpression.

(A) The expression levels of FGL1 and PD-L1 in four different natural cell lines were detected by quantitative PCR, $n = 3$. (B) Western blotting for FGL1, PD-L1, CD81, CD9, CD63, ALIX, and GAPDH in the whole cell lysate (WCL) and purified sEVs of HEK-293T, HepG2, A549, and MSC cells. (C) Schematic diagram of FGL1 and PD-L1 plasmid construction. The modified FGL1 constructs contains an artificial transmembrane domain (FGL1-TM), the coil-coil domain (CCD) and fibrinogen domain

(FD) of FGL1 (23-312aa) was fused with the FIBCD intracellular domain (IC) and transmembrane (TM) (1-57aa). SP represents signal peptide; ECD represents the extracellular domain. PD-L1 plasmid has the transmembrane structure of TM. (D) HEK-293T, HepG2, A549 and MSC cells stably expressing FGL1/PD-L1 were lysed by RIPA lysis buffer, and the expression of FGL1 and PD-L1 was detected by Western blot. (E) The expression of FGL1/PD-L1 on HEK-293T, HepG2, A549 and MSC cell membranes were observed by confocal microscope. Scale bar: 10 μm.

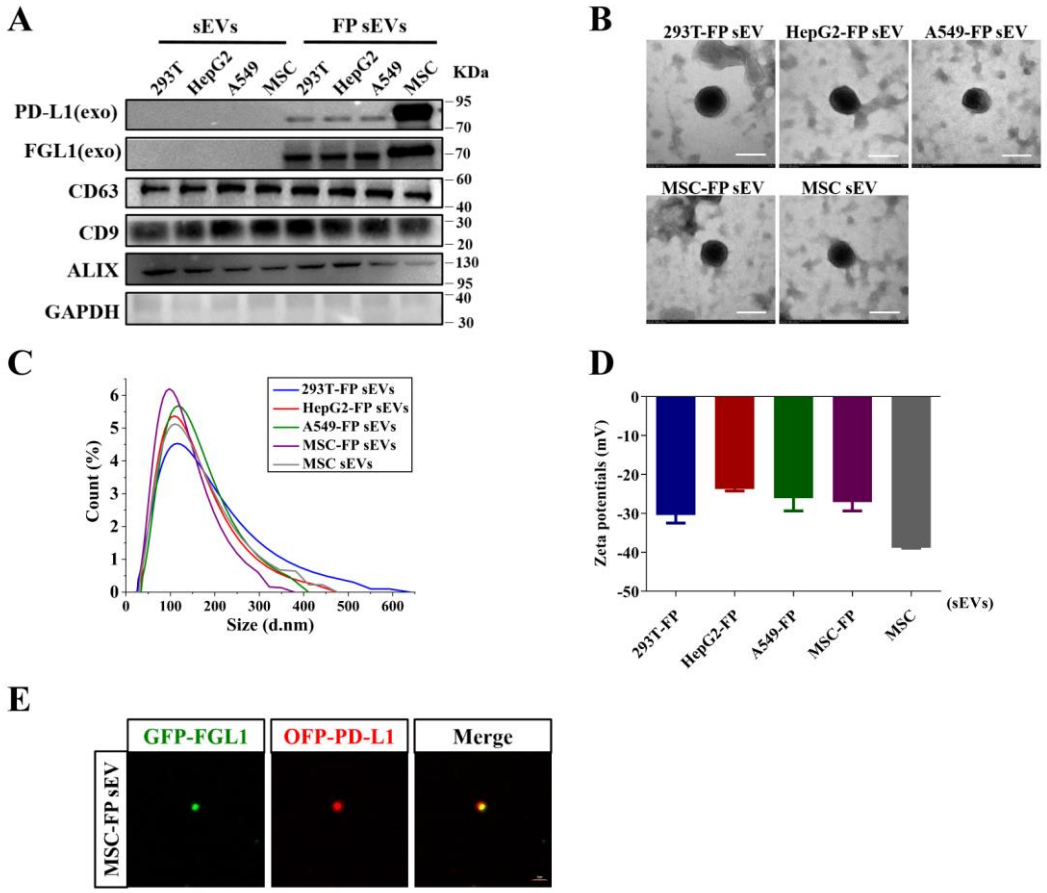

Figure 3. Establishment and characterization of FP sEVs and engineering MSC-FP can secrete modified exosomes delivering more FGL1/PD-L1.

(A) Western blotting for PD-L1 and FGL1 in the sEVs from HEK-293T, HepG2, A549, and MSC cells and overexpressed- FGL1/PD-L1 of these cell lines. (B-D) The TEM images (B), size distribution (C), and the Zeta potential (D) of purified sEVs from HEK-293T-FP, HepG2-FP, A549-FP， MSC-FP and MSC cells, $n = 3$. (E) Confocal images show the existence of FGL1-GFP/PD-L1-OFP on one sEV, scale bar: 2 μm.

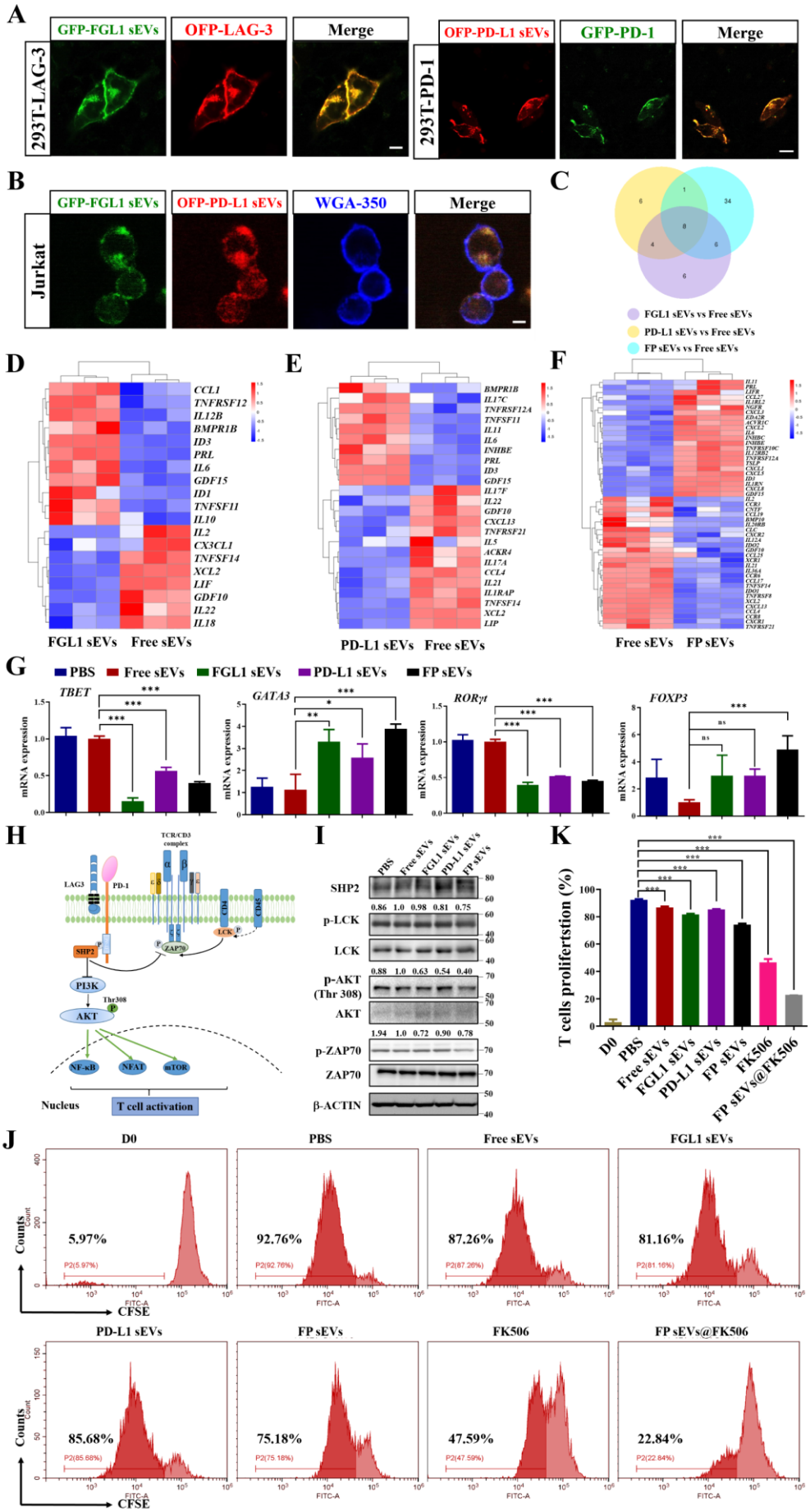

Figure 4. FGL1/PD-L1 sEVs could inhibite T cell proliferation and T cell function (A-B) FGL1, PD-L1, and FGL1/PD-L1 sEVs interacted with the membrane of LAG-3-OFP expressing HEK-293T cells, PD-1-GFP of HEK-293T cells (A), and PI-stimulated Jurkat cells (B) for 30 min, respectively. Scale bar: 10 μm. (C-F) Transcript abundance was measured via Illumina RNA-seq analysis of a VENN diagram (C) and heatmap (D-F) of cytokine-related gene expression in FGL1 sEVs vs Free sEVs (D), PD-L1 sEVs vs Free sEVs (E) and FP sEVs vs Free sEVs (F), $n = 3$. (G) Quantitative PCR to verify the expression of *TBET*, *GATA3*, *RORγt,* and *FOXP3* in PBMCs after treating with different sEVs groups, $n = 3$. (H) PD-1/LAG3 involved in the classic TCR signaling pathway. (I) Western blotting for TCR pathway protein expressions in Jurkat cells after treating with different sEVs groups. (J) Different groups inhibited the proliferation of $CD3^+$ T cells at 7 days shown using CFSE staining. $CD3^+$ T cells were stimulated with CD3 and IL-2. After 3 days, sEVs (50 μg/ml) were added to the cells for 7 days. CFSE staining was analyzed by flow cytometry. (K) The quantitative analysis of T cell proliferation after culture with different groups of sEVs, $n = 3$. Error bar, mean ± SD. $^*P < 0.05$, $^{**}P < 0.01$, $^{***}P < 0.001$.

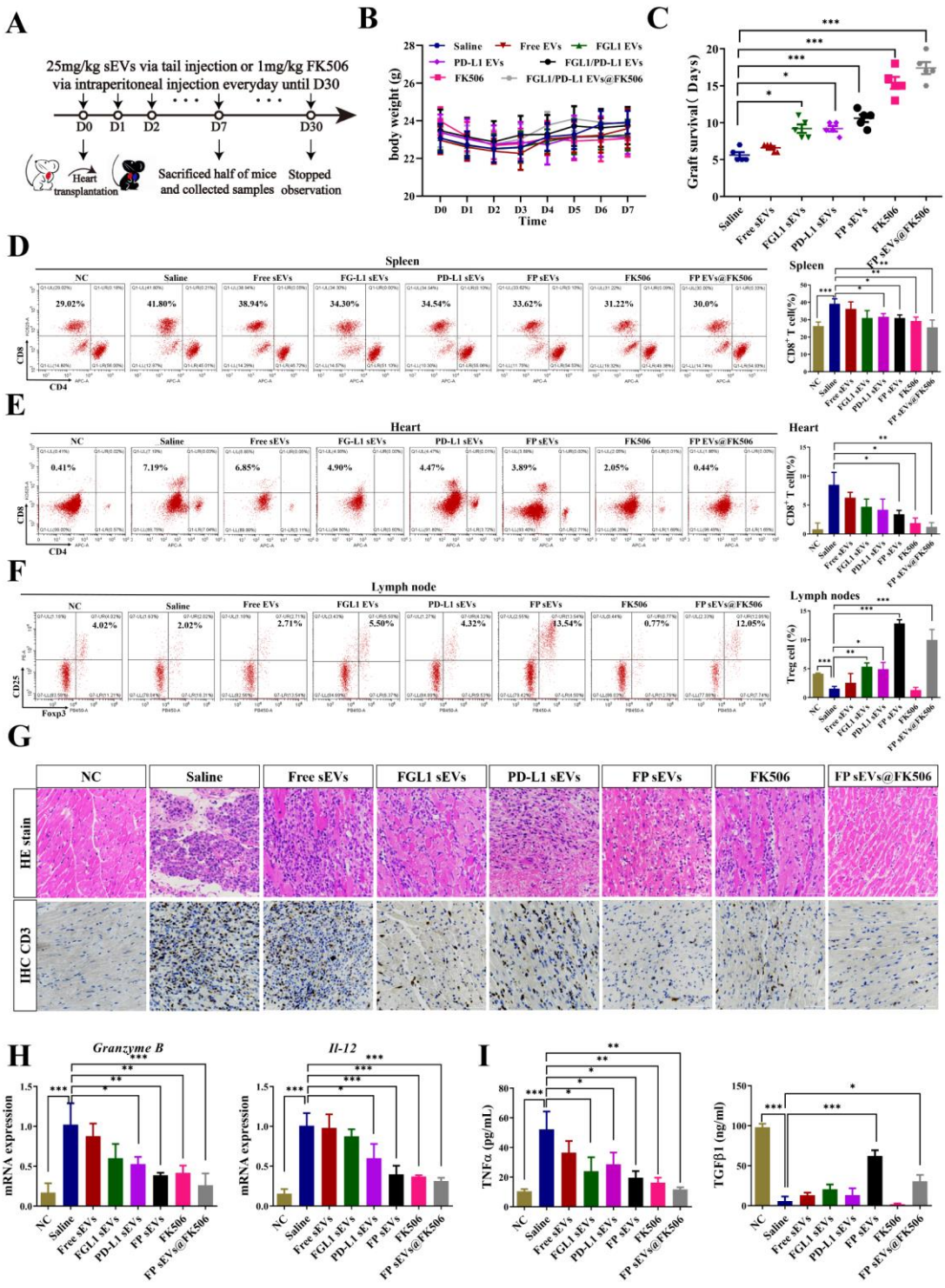

Figure 5. FGL1/PD-L1 sEVs promotes prolonged graft survival time and immune tolerance in a heart graft model.

(A) Images of the mode of administration of every group treatment. (B) The body weight of heat-graft mice in diverse groups as illustrated, $n = 5$. (C) Graft survival curves of cardiac allografts treated with different groups (Saline, Free sEVs, PD-L1 sEVs, FGL1 sEVs, FGL1/PD-L1 sEVs, FK506, FGL1/PD-L1 sEVs@FK506), $n = 5$. (D-E) Variation of CD8+ T cells in spleens (D) and hearts (E) were measured

by flow cytometry separately, n = 5. (F) Characteristic flow cytometry charts reveal changes of $CD4^+CD25^+Foxp3^+$ Treg cells in the superficial cervical lymph nodes of heart-transplanted mice, n = 3. (G) Hematoxylin-eosin (HE) staining and CD3-immunohistochemistry (IHC) show inflammation changes and quantity variance of infiltrated $CD3^+$ T cells in grafted-heart, respectively. Scar bar: 50 μm. (H) mRNA levels of cytokines for *Granzyme B* and *Il-12* using quantitative PCR, n = 5. (I) Secretion of cytokines for TNF-α and TGF-β1 in serum by ELISA, n = 5. Error bar, mean ±SEM. One-way ANOVA with Tukey's multiple comparisons test analyses were used. *$P < 0.05$, **$P < 0.01$, ***$P < 0.001$.

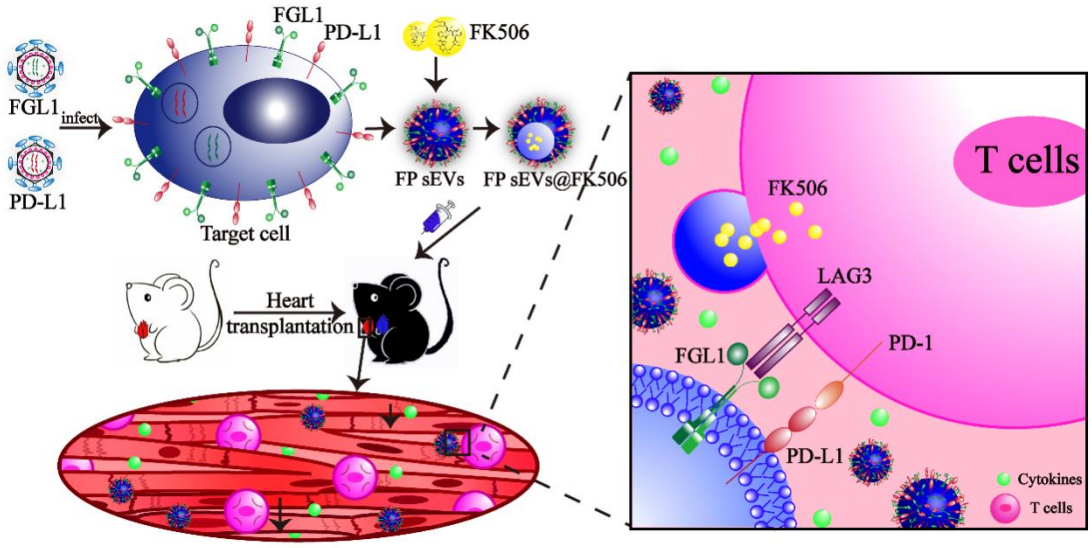

Figure 6. A schematic model showing FP sEVs@FK506 suppress T cell activation and thus inhibit cardiac allograft rejection.

FGL1 and PD-L1 packed with lentivirus successively infected target cells and thus were stably expressed upon cell surfaces. sEVs secreted by engineered cells stably expressed FGL1/PD-L1. At the same time, FK506, a classic immunosuppressant, was introduced into sEVs by electroporation. We translated the effects of FGL1/PD-L1 sEVs@FK506 onto a mouse heart-graft model to test their immunosuppressive function *in vivo*. FGL1/PD-L1 sEVs@FK506 administered by tail vein injection migrated to the grafted-hearts, causing a marked reduction in T cell activation and cytokine secretion. This was attributed to the blockage of the PD-L1/PD-1 and FGL1/LAG-3 axes, as well as the inhibitory effects of FK506 in immunological ejection.